processes

MDPI

Article

Preparation and Properties of Nano-Lignin-Reinforced Poly(butylene adipate-*co*-terephthalate) Composites

Yongshuang Li, Ting Feng, Jifei Liu, Cheng Pan, Yi Wang, Zhenzhen Wu * and Guozhi Fan *

Hubei Key Laboratory of Agricultural Waste Resource Utilization, School of Chemical and Environmental Engineering, Wuhan Polytechnic University, Wuhan 430023, China
* Correspondence: wuzhenzhen_200814@163.com (Z.W.); fgzcch@whpu.edu.cn (G.F.)

Abstract

The lignin nanoparticle (LNP) was prepared by the self-assembly method and further blended with poly(butylene adipate-*co*-terephthalate) (PBAT) to obtain a PBAT/LNP composite using a solvent casting method. It was found that the nano-modification of lignin effectively improved the compatibility between the components, and the mechanical properties, gas barrier properties, UV resistance, degradation, and antibacterial properties of the PBAT/LNP composite. Compared with PBAT, the tensile strength, elongation at break, and elastic modulus of the PBAT/LNP composite with 8 wt% LNP (PBAT/LNP-8) increased by 37.36%, 47.30% and 50.70%, respectively. Moreover, the mechanical properties, UV-blocking performance, and gas barrier properties of PBAT/LNP-8 were better than those of the commercial degradable packing bag, and the composite derived from PBAT and lignin extracted from wheat straw also showed excellent properties. This work explored a way to expand the utilization of lignin from lignocellulosic biomass, which not only helped to solve the environmental pollution caused by the widespread use of non-degradable plastics, but also promoted the replacement of fossil resources.

Keywords: lignin; nano-modification; poly(butylene adipate-*co*-terephthalate); biodegradable composite

check for updates

Academic Editor: Eduardo Vivaldo-Lima

Received: 18 September 2025
Revised: 19 October 2025
Accepted: 24 October 2025
Published: 1 November 2025

Citation: Li, Y.; Feng, T.; Liu, J.; Pan, C.; Wang, Y.; Wu, Z.; Fan, G. Preparation and Properties of Nano-Lignin-Reinforced Poly(butylene adipate-*co*-terephthalate) Composites. *Processes* **2025**, *13*, 3507. https://doi.org/10.3390/pr13113507

Copyright: © 2025 by the authors. Licensee MDPI, Basel, Switzerland. This article is an open access article distributed under the terms and conditions of the Creative Commons Attribution (CC BY) license (https://creativecommons.org/licenses/by/4.0/).

1. Introduction

Petroleum-based plastics have been widely applied in many fields due to their convenience and versatility, but they also aggravate the problems of resource consumption, energy shortages, and environmental pollution. Biodegradable plastic is considered to be an effective way to solve these problems, which not only reduces the reliance on fossil resources but also avoids environmental pollution.

Poly(butylene adipate-*co*-terephthalate) (PBAT) is a petroleum-based biodegradable polyester derived from the polycondensation of 1,4-butanediol, adipic acid, and terephthalic acid. It has superior biodegradability of aliphatic polyesters and favorable mechanical properties of aromatic polyesters [1], thus attracting wide attention in biodegradable plastics. However, the high cost of PBAT limits its wide application [2]. The incorporation of low-cost fillers is one of the important ways to reduce the cost of PBAT-based composites [3], which is also expected to improve material properties.

Lignocellulose is the most abundant biomass in the world and is considered to be a source of high-value chemicals [4]. It has been reported that lignocellulosic components can be used as a reinforcing agent. The incorporation of these components into biodegradable materials not only reduces the cost but also enhances the comprehensive

properties [5–7]. Lignin is one of the main components of lignocellulose and a common by-product of the biomass refining industry. Generally, the majority of lignin is used as fuel for combustion or directly discarded, while only a small amount is used to develop high-value products [8]. It is necessary to explore high-value utilization of lignin in terms of resource utilization efficiency.

Lignin has been used as a filler for the PBAT matrix composites. Ethyl acetate-dissolved lignin (EL) with a low molecular weight and low glass transition temperature was obtained by using organic solvent fractionation and was further used to prepare EL/PBAT composites by blending with PBAT. It was found that there were strong intermolecular interactions between PBAT and EL [9]. The composites still had higher tensile strength (σ) (24.7 MPa) and elongation at break (ε) (494.7%) even in the presence of 50 wt% EL. Moreover, compared with PBAT, the yield strength and elastic modulus (E) increased by 200% and 768%, respectively, and the cost decreased by 22.9%. Since a large number of polyphenols, quinone structures, and hydroxyl groups are contained in lignin molecules, strong intermolecular forces and easy agglomeration result in poor compatibility between lignin and polymers [10,11]. Therefore, the modification of lignin through chemical or physical methods is usually required. For example, vinyltrimethoxysilane-grafted lignin (VL) was blended with PBAT to prepare PBAT/VL composites; the mechanical properties and biodegradation rate were significantly improved, and the σ, E, and biodegradation rate increased by 200%, 151% and 96%, respectively [12]. Lignin and tannic acid were encapsulated in epoxidized soya bean oil and further blended with PBAT to prepare composites by the solvent casting method. Both the σ and the gas barrier property of the composites were improved due to the addition of filler. The σ increased by 132% and a reduction in water vapor and oxygen transmission was observed; furthermore, it prolonged the food shelf-life [13].

The lignin nanoparticle (LNP) has high stability and activity, as well as good biocompatibility and biodegradability [14]. It can reinforce polymer properties, including thermal stability, degradation efficiency, optical, mechanical, and permeability properties [15]. LNP/polylactic acid (PLA) composites were obtained by combining solvent casting and melt blending methods. The mechanical properties, the nucleation, and the oxidation resistance of the composites were improved due to the addition of LNP. Compared to PLA, the σ and E increased by 184% and 115%, respectively, in the presence of 2.5 wt% LNP [16]. Hydrophobic lignin-based nanospheres (LNSs) obtained by the self-assembly method were blended with poly(vinyl alcohol) (PVA) solution to prepare LNSs/PVA composites. The incorporation of LNSs enhanced the mechanical properties, thermal stability, UV resistance, and biodegradation of the composites. The σ and E values of the composites increased by 47.4% and 81.2%, respectively, due to the addition of 4 wt% LNSs [17].

LNP was also employed to prepare PBAT-based composites. The incorporation of LNPs prepared via antisolvent precipitation from softwood Kraft lignin into PBAT matrices was also investigated. LNPs acted as functional fillers, exhibiting excellent dispersion within the PBAT matrix. The mechanical properties of the composite were significantly improved, and the σ increased 62.1% [18]. Generally, Kraft lignin was used as the filler [18,19]. Since the structure and properties of lignin are affected by the source, it is also necessary to explore the application of other types of lignin, such as dealkaline lignin (DL), in the field of biodegradable materials. Agricultural wastes, including straw and bamboo, are considered to be one of the main sources of DL, and the research on DL is expected to expand the application of agricultural waste.

Herein, LNP from DL was simply prepared by an ultrasonic-assisted self-assembly method and further blended with PBAT to prepare PBAT/LNP composites using the solvent casting method. The effects of LNP content on the mechanical properties, thermal

stability, hydrophobicity, and gas barrier properties were investigated. The UV-blocking property, degradation process, and antibacterial property of the composite were also explored. Furthermore, the comprehensive properties of the composite were compared to those of the commercial degradable packing bag (CDBP). The PBAT/LNP composite was also prepared by blending lignin extracted from wheat straw with PBAT. This work supplied a potential way for the application of lignocellulosic biomass in the degradable packing materials field.

2. Materials and Methods

2.1. Materials

DL was purchased from Aladdin Biochemical Technology Co., Ltd. (Shanghai, China). Ethyl acetate, trichloromethane ($CHCl_3$), *N*, *N*-dimethylacetamide (DMAc), sodium chloride (NaCl), potassium chloride (KCl), sodium hydrogen phosphate (Na_2HPO_4), potassium phosphate monobasic (KH_2PO_4), and hydrochloric acid (HCl) were purchased from Sinopharm Chemical Reagent Co., Ltd. (Beijing, China). *Escherichia coli* (*E. coli*) and *Staphylococcus aureus* (*S. aureus*) were purchased from Shanghai Luwei Technology Co., Ltd. (Shanghai, China). PBAT (Th801t, Mw: 7.50 × 104 g/mol) was purchased from Xinjiang Blue Ridge Tunhe Sci. & Tech. Co., Ltd. (Changji, China). The wheat straw lignin (WSL) was extracted according to our previous work [20,21], and the CDBP was purchased from a local supermarket.

2.2. Preparation of LNP

Typically, 1 g DL and 40 mL ethyl acetate were added to a 500 mL beaker, followed by ultrasonic dispersion for 20 min. Then, 100 mL of deionized water was added dropwise for about 2 h. The mixture was stirred at room temperature for 4 h before concentrating at 80 °C. The solid was collected and freeze-dried for 24 h to obtain LNP [22].

2.3. Preparation of PBAT/LNP Composite

Typically, 0.08 g LNP and 15 mL DMAc were added into a 100 mL three-necked flask, followed by stirring at 60 °C for 0.5 h. Then, 0.92 g PBAT and 10 mL $CHCl_3$ were added, and the mixture was continually stirred at 60 °C for 1 h. The mixture was poured into a Petri dish and covered with plastic wrap with small holes, followed by standing for 15 h and freeze-drying at 60 °C for 12 h to obtain PBAT/LNP composite, denoted PBAT/LNP-8 (8 wt% LNP in the composite). Finally, by varying the content of LNP, a series of composites with 5 wt%, 6 wt%, 7 wt%, 9 wt%, 10 wt%, and 11 wt% LNP was prepared. They were denoted PBAT/LNP-5, PBAT/LNP-6, PBAT/LNP-7, PBAT/LNP-9, PBAT/LNP-10, and PBAT/LNP-11, respectively. WSL was nano-modified by the same method as DL, and nano-WSL reinforced PBAT was prepared by the same procedure as that of the PBAT/LNP composite.

2.4. Measurement of Composite Properties

2.4.1. Mechanical Properties

The mechanical properties of the composites were determined by an XLW intelligent electronic tensile tester (Labthink, Jinan, China) according to ISO 527-4-2021 [23]. The drawing speed and the fixture spacing are 50 mm/min and 50 mm, respectively. The tensile stress–strain curves were the averages of five measurements, and the value of *E* was calculated according to Equation (S1).

2.4.2. Thermal Properties

The thermogravimetric analysis (TGA) of the composites was performed on a TGA 8000 thermogravimetric analyzer (PerkinElmer, Waltham, MA, USA) under a nitrogen atmosphere at a heating rate of 10 °C/min in the range of 30–800 °C.

2.4.3. Water Contact Angle

The water contact angle (WCA) of the composites was measured on a Dataphysics OCA 25 contact angle tester under static conditions. The composite sample was attached to a glass slide, and 2 μL of distilled water was dropped on the surface of the sample. Then, the WCA was measured and repeated three times.

2.4.4. Water Vapor Transmission

The water vapor transmission (WVT) of the composites was estimated according to ASTM E-96-95 [24]. The composite was cut into a circle with a diameter of 6 cm, followed by sealing in a Petri dish containing 25 g of distilled water. The Petri dish was then kept at 23 °C with 50% relative humidity, and weighed every 30 min. The WVT was calculated according to Equation (S2).

2.4.5. Oxygen Permeability

The oxygen permeability (OP) of the composites was determined using a VAC-VBS gas permeability tester (Labthink, Jinan, China) with the differential pressure method [25]. The ambient temperature was 23 °C and the relative humidity was 50%. The composite sample was cut into a circle of 6 cm in diameter and fixed on the permeation unit with an exposure area of 38 cm^2. The measurement was repeated three times, and the OP was calculated according to Equation (S3).

2.4.6. UV-Blocking Performance

The light transmission of the composites was determined by a TU-1901 double-beam UV-vis spectrophotometer. A sample was cut into 1 cm × 3 cm portions and attached to the surface of the cuvette. The absorbance was measured in the range of 200–1100 nm, and an empty cuvette was used as a blank control.

2.4.7. Degradation Test

The samples were cut into 2 cm × 3 cm portions, dried at 60 °C for 4 h prior to weighing. The samples were placed in a Petri dish containing natural soil, with a moisture content of 33.23 ± 7.76% and a pH of 7.4 ± 0.3. The buried samples were taken out every 10 d, washed with distilled water, dried at 60 °C for 8 h, weighed, and then buried in the soil. The biodegradation rate was the average value of three samples [26] and calculated according to Equation (S4).

2.4.8. Antibacterial Property

The antibacterial property of the composites was determined according to the reported procedure [1]. Typically, 8 g NaCl, 0.2 g KCl, 1.44 g Na_2HPO_4, and 0.24 g KH_2PO_4 were dissolved in 900 mL of distilled water. The pH value of the mixture was adjusted to 7.4 with 1 wt% HCl solution and then diluted to 1 L with distilled water. Phosphate-buffer solution (PBS) was obtained and used as the control group. A single colony of *E. coli* or *S. aureus* was added to 50 mL liquid medium, followed by culturing at 37 °C for 12 h to obtain a bacterial solution. The PBAT/LNP-8 composite was cut into a sample of 2 cm in diameter and irradiated with UV light, then the sample was put into the mixture of 20 μL of the bacterial solution and 50 mL PBS, followed by cultivating at 37 °C for 3 h to obtain the bacterial culture solution.

2.5. Calculation and Statistical Analysis

The values of E, WVT, OP, and biodegradation rate were calculated according to Equations (S1)–(S4). All data were presented as mean ± standard deviation. The mean differences were determined by statistical analysis of the data performed using analysis of variance (ANOVA) and Origin software, followed by Duncan's multiple range test. Statistical significance was set at a level of $p < 0.05$ [6,27].

2.6. Measurements

FTIR was performed on a Thermo Nicolet 330 Fourier transform infrared spectrometer (ThermoFisher, Waltham, MA, USA) in the range of 500–4000 cm^{-1}. The particle size distribution was determined by a Mastersizer 2000 (Micromeritics, Norcross, GA, USA) laser particle size analyzer using water as the dispersant in the range of 0–500,000 nm. XRD was conducted using a Bruker D8 Advance X-ray diffractometer (Bruker, Billerica, MA, USA) with Kα rays, Cu target, λ = 1.5406 Å, tube voltage and tube current of 40 kV and 40 mA, respectively, with scanning speed of 6°/min, and a scanning range of 2θ = 10–80°. The sample morphology was analyzed with a Zeiss Gemini 300 scanning electron microscope (Zeiss, Oberkochen, Baden-Württemberg, Germany), gold spray treatment, acceleration voltage of 15 kV, and a cold field-emission electron source.

3. Results and Discussion

3.1. Characterization

3.1.1. Characterization of LNP

The FTIR spectra of DL and LNP are shown in Figure 1a. In the FTIR spectrum of DL, the band at 3430 cm^{-1} was caused by the stretching vibration of the intramolecular –OH groups. The bands at 2930 cm^{-1} and 2854 cm^{-1} belonged to the asymmetric stretching vibration of C–H in methyl and the symmetric stretching vibration of C–H in $–CH_2$, respectively [28,29]. The bands at 1623 cm^{-1} and 1463 cm^{-1} were attributed to the stretching vibrations of the *p*-hydroxyphenyl structural unit [30]. The bands at 1513 cm^{-1}, 860 cm^{-1}, and 820 cm^{-1} were caused by the vibrations of C–C stretching in the benzene ring, and the band at 1269 cm^{-1} was ascribed to the stretching vibration of C–O [31]. All these bands were the characteristic absorption bands of lignin. The characteristic absorption bands of LNP were similar to those of DL. Therefore, it is reasonable to conclude that the functional groups and chemical structure of DL did not change significantly during the modification, which was a physical process.

The particle sizes of DL and LNP were analyzed, as shown in Figure 1b. The particle size of DL was mainly distributed in the range of 40–220 μm. After modification, the particle size was significantly reduced, and the particle size of LNP was mainly distributed in the range of 140–340 nm. This is due to the fact that lignin is difficult to dissolve in the water phase. To reduce the interfacial energy, lignin gradually tends to form a curvature structure in the coexistence solvent of ethyl acetate and deionized water [20], which leads to lignin self-assembly to form LNP.

3.1.2. Characterization of PBAT/LNP Composite

FTIR

Figure 2a shows the FTIR spectra of PBAT and its composites. In the FTIR spectrum of PBAT, the band at 3430 cm^{-1} was caused by the stretching vibration of –OH groups. The bands at 2960 cm^{-1} and 2860 cm^{-1} were ascribed to the asymmetric stretching vibration of C–H in methyl and the symmetric stretching vibration of C–H in methylene, respectively [32]. The bands at 1720 cm^{-1} and 1270 cm^{-1} belonged to the stretching vibrations of C=O and C–O in the ester chain, respectively [33], and the band at 1510 cm^{-1} was attributed

to the backbone vibration of the benzene ring in PBAT [34]. In the spectra of PBAT/LNP composites, the band at 3430 cm^{-1} attributed to –OH significantly became wider. It was due to the fact that the formation of intermolecular hydrogen bonding between the hydroxyl groups in LNP and the ester groups in PBAT [34,35]. Furthermore, a new band at 1630 cm^{-1}, belonging to the bending vibration of adsorbed water, was observed. Since a large number of hydrophilic groups are contained in LNP, the introduction of LNP facilitated the formation of hydrogen bonding between the composites and water molecules, thus enhancing the hydrophilicity of the composites. In the FTIR spectra of PBAT/LNP composites, the band at 2930 cm^{-1} ascribed to LNP was not observed. It may be covered by the band at 2960 cm^{-1} caused by PBAT due to the low content of LNP in the composites. It can also be seen from Figure 2 that the addition of LNP had little effect on the FTIR spectra of the composites. The FTIR spectra of PBAT/LNP composites with different LNP contents were similar, indicating that LNP and PBAT were only physically blended.

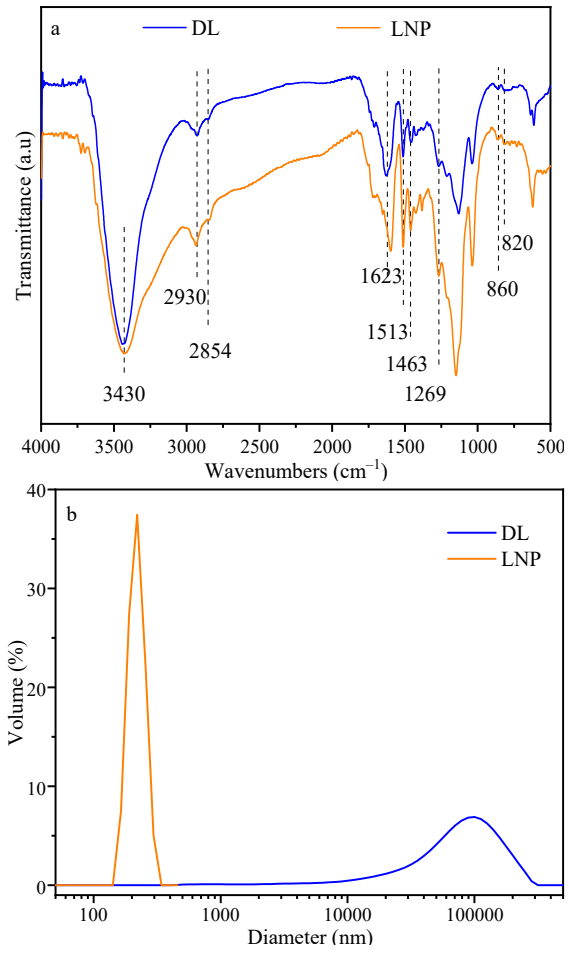


Figure 1. (**a**) FTIR spectra and (**b**) particle size distributions of DL and LNP.

The FTIR spectra of the PBAT/LNP-8 composite and its degraded samples are shown in Figure 2b. The characteristic bands at 3430 cm^{-1} and 1630 cm^{-1}, attributed to –OH and adsorbed water, were significantly enhanced, while the characteristic bands at 2960 cm^{-1}, 2860 cm^{-1}, 1720 cm^{-1}, 1270 cm^{-1}, and 1510 cm^{-1}, belonging to PBAT, became weaker. These results suggested the degradation of PBAT during soil burial, leading to the cleavage of the ester bond and the formation of oligomeric residues. Therefore, the hydroxyl sites increased, and the characteristic band belonging to –OH was strengthened. It improved the water absorption of the composites and displayed a positive effect on further degradation of PBAT. Moreover, the band at 2930 cm^{-1} ascribed to LNP reappeared after

degradation for 60 d, further suggesting that the ester chain in PBAT was broken during the degradation process.

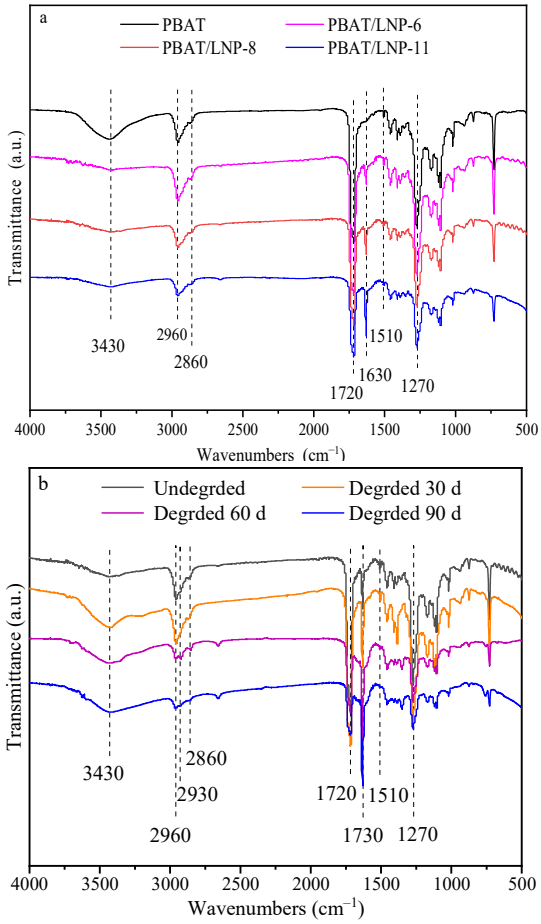


Figure 2. FTIR spectra of (**a**) PBAT and PBAT/LNP composites and (**b**) PBAT/LNP-8 degradation samples.

XRD

The XRD pattern of PBAT and its composites is shown in Figure 3a. In the XRD pattern of neat PBAT, the characteristic diffraction peaks at 17.4°, 20.5°, and 23.1° corresponded to PBAT crystal planes (010), (110), and (100), respectively [36]. In the XRD patterns of PBAT/LNP composites, in addition to the characteristic diffraction peaks of PBAT, weak peaks at 31.8°, 33.9°, 39.3°, and 46.3° ascribed to LNP also appeared [37]. Furthermore, the intensities of the diffraction peaks attributed to PBAT increased, indicating that the addition of LNP improved the crystallinity of PBAT. The results in Table S1 showed that the crystallinity of the neat PBAT was 26.87% while that of the PBAT/LNP composites varied in the range of 41.03% to 46.58%. This is can be explained by the following reasons: firstly, the crystallinity of the composite was enhanced by the incorporation of rigid filler of lignin [38]; secondly, the LNP particle with aromatic structure was able to act as the nucleating agent for semicrystalline polymers (such as PBAT) with an aromatic ring in their backbones through π-π interactions [39]; thirdly, the interaction between the hydroxyl group of LNP and the ester group of PBAT promoted the formation of intermolecular hydrogen bond (Figure 2a), which also caused an increase in the crystallinity of the composite [40]. Therefore, the crystallinity of PBAT/LNP increased with increasing LNP addition. As the crystallinity of the composites increased, the mechanical and barrier properties could be enhanced [41]. So it is reasonable to speculate that the LNP content in the composite may affect its comprehensive performance.

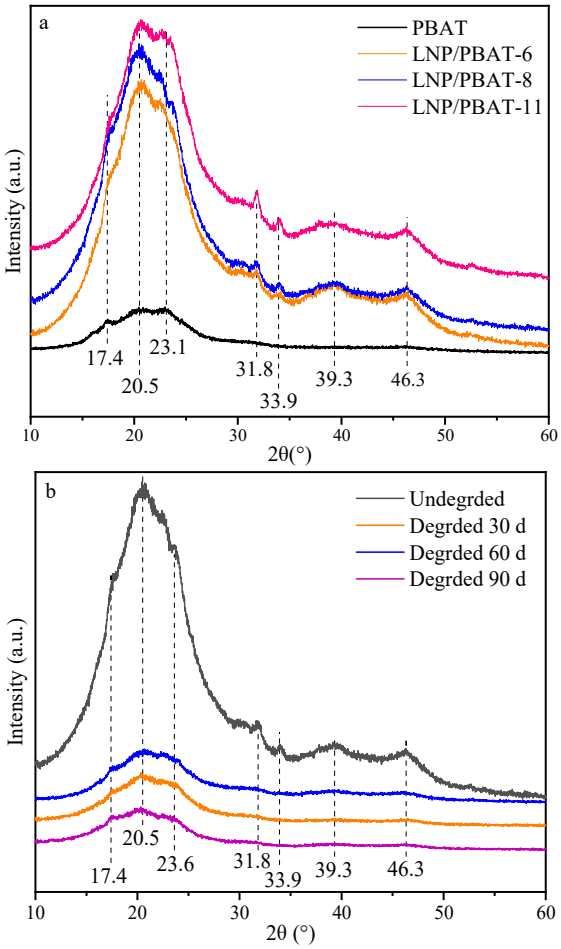


Figure 3. XRD patterns of (**a**) PBAT and PBAT/LNP composites and (**b**) PBAT/LNP-8 degradation samples.

The XRD patterns of PBAT/LNP-8 and its degraded samples are shown in Figure 3b. Compared to the undegraded sample, the intensities of the characteristic diffraction peaks attributed to both PBAT and LNP decreased. The results in Table S1 indicated that the crystallinity of the PBAT/LNP-8 composite was decreased from 46.58% to 26.54% after degrading 90 d. Combining the FTIR results in Figure 2b, it is further evident that both LNP and PBAT underwent degradation in the soil. The above-mentioned factors, such as the nucleation effect of LNP and the interaction between LNP and PBAT, were reduced. It affected the crystallization behavior of the components in the composites.

SEM

The morphologies of PBAT and PBAT/LNP-8 were observed by SEM, and the results are shown in Figure 4. According to Figure 4a, the surface of PBAT was relatively smooth and flat with a continuous homogeneous phase. After incorporating LNP, the surface of the PBAT/LNP-8 composite still remained smooth (Figure 4b), indicating the uniform dispersion of LNP in PBAT without obvious agglomeration and good compatibility between PBAT and LNP. This can be ascribed to LNP has high stability and good biocompatibility [14]. Therefore, it is reasonable to conclude that the addition of LNP may enhance the comprehensive properties of the composites. However, Figure 4b also showed the presence of particles on the surface of PBAT/LNP-8 and slight differences in the morphologies at various magnifications, suggesting that the dispersion of LNP in PBAT can be further improved.

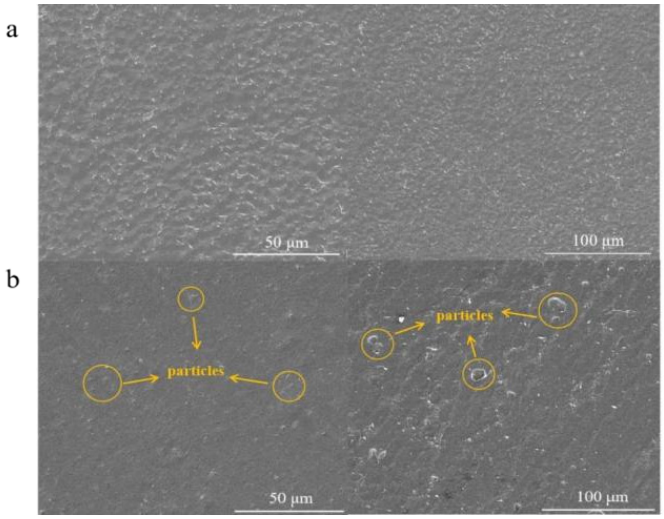


Figure 4. SEM images of (**a**) PBAT and (**b**) PBAT/LNP-8 composite.

The morphologies of the PBAT/LNP-8 composite and its degraded samples are shown in Figure 5. After degradation for 30 d, the surface of the composite became rougher (Figure 5a). It can be ascribed to the degradation of PBAT and LNP in the presence of microorganisms in soil, as the results of IR in Figure 2b and XRD in Figure 3b. Additionally, the particles on the surface of the composite became more obvious, suggesting that PBAT and LNP had different degradation rates. According to Figure 5b, after degradation for 60 d, the surface of the PBAT/LNP-8 composite, contrarily, became smoother. However, obvious holes can be observed, which may be caused by a higher degradation rate of LNP on the surface of the composite. Since LNP doped in the PBAT matrix degraded first, which promoted the formation of the holes. Figure 5c showed that almost no particles appeared on the surface of the composite after degradation for 90 d, indicating complete degradation of LNP.

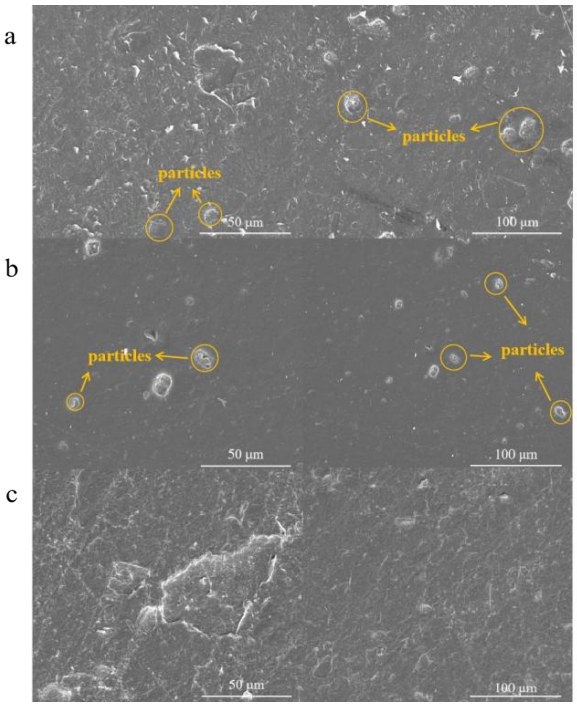


Figure 5. SEM images of PBAT/LNP-8 degraded samples for (**a**) 30 d; (**b**) 60 d; (**c**) 90 d.

3.2. Properties of Composites

3.2.1. Mechanical Properties

The stress–strain curves and mechanical properties of PBAT and its composites are shown in Figure 6. According to Figure 6a, the maximum yield stress of PBAT was 6.26 MPa. As the content of LNP increased, the yield stress of PBAT/LNP composites first increased and then decreased in the range of 5.93 MPa to 9.67 MPa. The maximum yield stress of 9.67 MPa was obtained with 8 wt% LNP content; it increased by 54.47% compared to that of PBAT. The incorporation of LNP enhanced the stiffness of the composites due to its high rigidity [42].

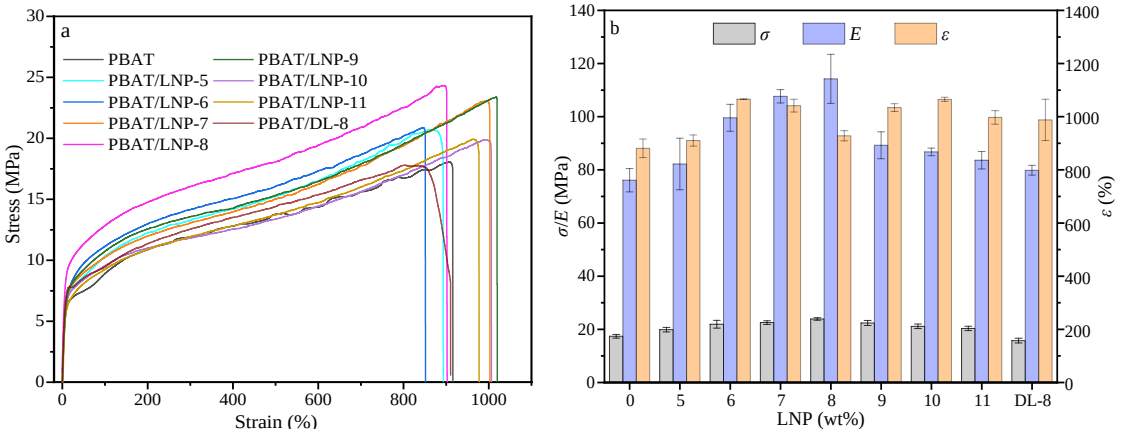


Figure 6. (**a**) Stress–strain curves and (**b**) mechanical properties of PBAT and PBAT/LNP composites.

Figure 6b illustrates that the σ, ε, and E of PBAT were 17.37 MPa, 880.90% and 76.11 MPa, respectively. As the content of LNP increases, the σ and E of PBAT/LNP composites first increased and then decreased in the ranges of 19.87 MPa–23.86 MPa and 82.20 MPa–114.22 MPa, respectively. It was evident that they were always higher than those of PBAT. The PBAT/LNP-8 composites with 8 wt% LNP exhibited relatively excellent mechanical properties, and the σ, ε, and E were 23.86 MPa, 928.20%, and 114.22 MPa, respectively. They increased by 37.36%, 47.30%, and 50.70% compared to those of PBAT, respectively. Further increase in the content of LNP instead resulted in a decrease in the σ and E, but the ε varied in the range of 928.2% to 1065.2%. The σ and E decreased to 20.33 MPa and 83.61 MPa, respectively, in the presence of 11 wt% LNP. These results indicated that the mechanical properties of the composites increased with the increase in the LNP content. However, excessive LNP molecules resulted in the intermolecular agglomeration [43], which caused a strong stress concentration effect and phase separation between lignin and PBAT. As a result, the stress transfer on macromolecular PBAT was interrupted [44], and the σ and E of the composite decreased.

PBAT/DL composite with 8 wt% DL was also prepared, and the σ, ε, and E were 15.73 MPa, 987.9%, and 79.83 MPa, respectively. Compared with PBAT/LNP-8, the ε was close, but the σ and E decreased by 51.68% and 43.08%, respectively. This was attributed to the fact that the particle size of lignin was reduced by the nano-modification, which improved the compatibility between lignin and PBAT, as shown in Figure 5. These results suggested that the strength of the composites was enhanced by the incorporation of LNP, while good toughness was maintained. It is expected that the composite will have excellent processing performance, thus expanding the application of PBAT in the packaging field.

3.2.2. Thermal Properties

The TGA-DTG curves of PBAT and its composites are shown in Figure 7. According to Figure 7a, the thermal decomposition of PBAT began around 300 °C. The main weight

loss occurred in the range of 350 °C to 475 °C, giving a weight loss of 95.80 wt%. The main weight loss of the PBAT/LNP composites occurred in the range of 320 °C to 460 °C, and a slight decrease in the weight loss was observed with increasing LNP content. The weight loss of PBAT/LNP-6, PBAT/LNP-8, and PBAT/LNP-11 was 90.24 wt%, 89.32 wt%, and 88.09 wt%, which were lower than that of PBAT. Therefore, the residuals of the PBAT/LNP composites increased with increasing the content of LNP. The residual amounts of PBAT, PBAT/LNP-6, PBAT/LNP-8, and PBAT/LNP-11 were 1.64 wt%, 5.88 wt%, 6.15 wt%, and 8.23 wt%, respectively. This is due to the high carbon content of lignin [45]. The DTG curves in Figure 7b showed that the maximum pyrolysis temperature of PBAT was 420 °C, and the maximum pyrolysis temperatures of PBAT/LNP composites varied in the range of 402 °C to 411 °C, indicating that the thermal stability of the composites was insignificantly affected by the addition of LNP. Surprisingly, the maximum pyrolysis temperatures of the PBAT/LNP composites were closer to that of PBAT with the increase in the content of LNP. The maximum pyrolysis temperatures of PBAT/LNP-6, PBAT/LNP-8, and PBAT/LNP-11 were 402 °C, 404 °C and 411 °C, respectively. This may be due to the fact that the intramolecular and intermolecular hydrogen bonding (Figure 2a) and π-π interactions were enhanced with increasing the LNP content in the composites [45]. It caused the agglomeration of LNP, and higher energy was required to disrupt intermolecular interactions [13]. Therefore, the maximum pyrolysis temperature of PBAT/LNP composite gradually increased with the increase in the LNP content.

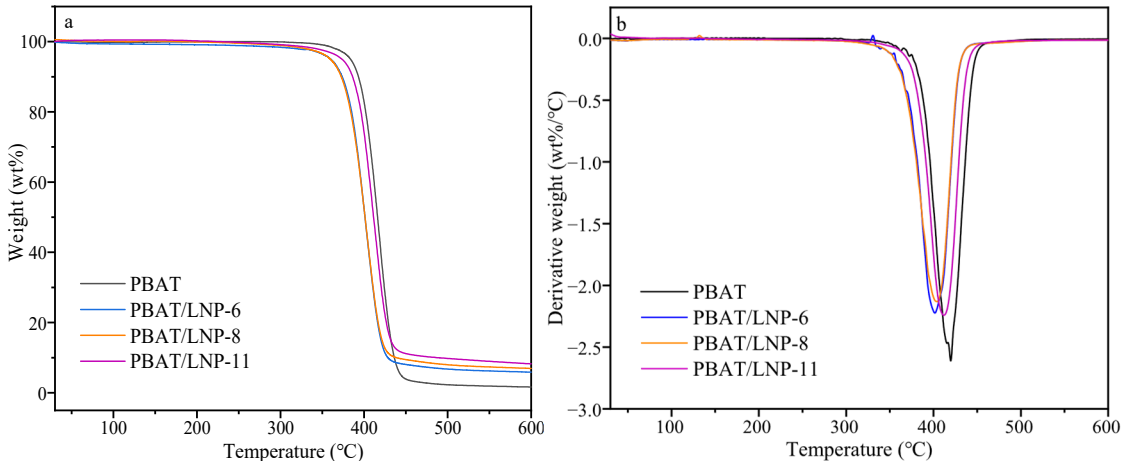


Figure 7. (**a**) TGA and (**b**) DTG curves of PBAT and PBAT/LNP composites.

3.2.3. WCA

Figure 8 shows the WCA of PBAT and its composites. Since PBAT was hydrophobic, a WCA of 90.1° was observed. It is well-known that hydroxyl groups and ester groups are contained in LNP and PBAT, respectively, and they form intermolecular hydrogen bonds [34,35], as shown in Figure 2. Therefore, the hydrophilicity of the composites was improved due to the addition of LNP, increasing with the increase in the content of LNP. The WCA of the composites decreased from 86.4° to 76.5° with increasing the content of LNP from 5 wt% to 11 wt%.

3.2.4. Gas Barrier Properties

Figure 9 shows the gas barrier properties of PBAT and its composites. The WVT of PBAT was 47.24 g/(m^2·24 h), and the WVT of the composites was enhanced after the addition of LNP (Figure 9a). Moreover, the WVT of the composites increased with increasing the content of LNP in the range of 5 wt% to 11 wt%. It was enhanced from 48.83 g/(m^2·24 h) to 53.44 g/(m^2·24 h). The results further indicated that the addition of

LNP improved the hydrophilicity of the composites, which was in agreement with the results of WCA in Figure 8. According to Figure 2, the hydrophilic hydroxyl groups in LNP promoted the formation of hydrogen bonds in the PBAT/LNP composite. As a result, the interaction between the composite with water molecules was enhanced, facilitating the diffusion of water and improving the hydrophilicity of the composite.

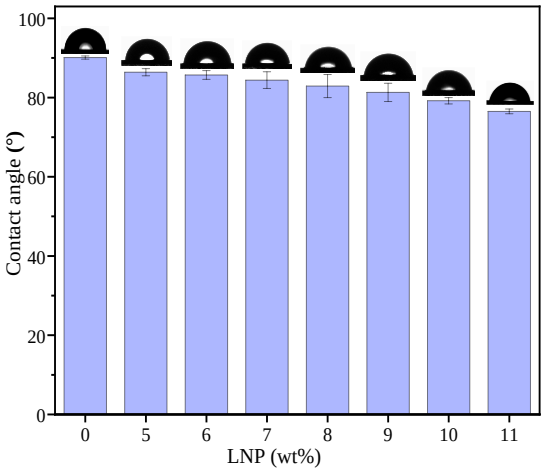


Figure 8. WCA of PBAT and PBAT/LNP composites.

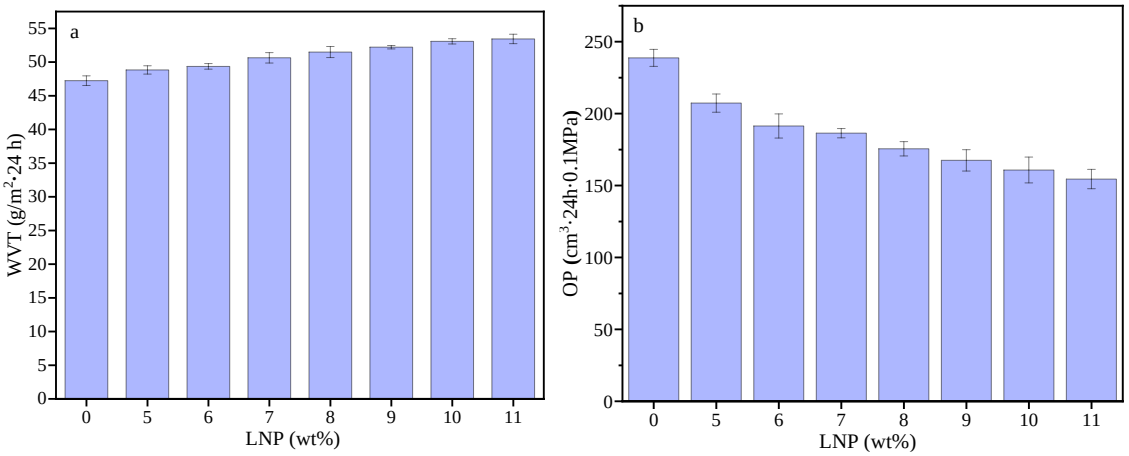


Figure 9. (**a**) WVT and (**b**) OP of PBAT and PBAT/LNP composites.

Figure 9b shows the OP of PBAT and its composites. The OP of PBAT was 238.76 cm^3/(24 h·0.1 MPa), and the OP of the composites gradually decreased after the addition of LNP. When the LNP content was increased from 5 wt% to 11 wt%, the OP of the composite decreased from 207.30 cm^3/(24 h·0.1 MPa) to 154.47 cm^3/(24 h·0.1 MPa). It was found that the gas permeation is greatly dependent on the diffusion process of the gas through the polymer [46]. Due to the good compatibility between LNP and PBAT, LNP can be uniformly dispersed in the composite (Figure 4). After the incorporation of LNP, the internal structure of the composites became more complex, which made the diffusion of oxygen more difficult, thus improving the oxygen barrier properties.

3.2.5. UV-Blocking Performance

The photodegradation caused by UV irradiation is the main factor for the rapid aging of PBAT [47]. Lignin is considered to be a natural broad UV blocker to screen almost the whole spectrum of UV light due to phenolic units, ketones, and chromophores in its structure [48]. Therefore, the UV-blocking performance of the composites may be enhanced due to the incorporation of LNP. The light transmittance of PBAT and its composites was

measured in the UV-light region, and the results are shown in Figure 10. In the UVA region of 320 to 400 nm, PBAT had poor UV-blocking performance with a light transmittance of 44.9–10.5%. In the UVB region of 275 nm to 320 nm and UVC region of 200 nm to 275 nm, the UV light was almost completely absorbed. This is due to its benzene rings and carbonyl groups, which absorb photon energy and convert it to heat [15,48].

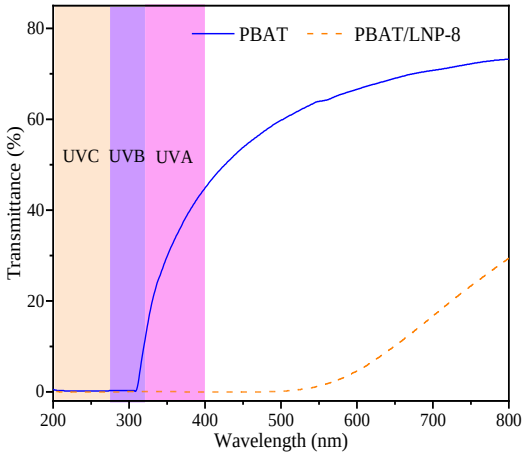


Figure 10. UV-blocking performance of PBAT and PBAT/LNP-8.

According to Figure 10, the PBAT/LNP-8 composite exhibited excellent UV-blocking performance; the UV lights in all regions, including UVA, UVB, and UVC, were completely shielded, confirming that the UV-blocking performance of the composites was enhanced by the incorporation of LNP. This was conducive to prolonging the service life of the composites. Additionally, PBAT/LNP-8 composites also exhibited good shielding performance in the visible light region of 400 nm to 800 nm, and the maximum light transmittance was only 29.4%. Therefore, the PBAT/LNP-8 composites can be expected to apply in light-sensitive product packaging.

3.2.6. Biodegradation Property

The biodegradation of PBAT and PBAT/LNP-8 was performed by the soil burial biodegradation test, and the results are shown in Figure 11. Due to a few microorganisms that can degrade PBAT in soil [46], the degradation of PBAT was slow, and only a 2.31% biodegradation rate was observed after 90 d. The addition of LNP improved the biodegradation rate of PBAT/LNP-8 composite. The degradation rate was enhanced to 5.83%, which was 2.52 times higher than that of PBAT. It can be attributed to two factors. Combining Figures 3b and 4, it was evident that the degradation of LNP was easier than that of PBAT. Additionally, the breakage of the ester bond of PBAT led to the formation of new hydroxyl sites. It enhanced the water absorption capacity of the composite (Figure 2b) during the degradation, thus further accelerating the degradation of PBAT and enhancing the biodegradation rate.

3.2.7. Antibacterial Property

The antibacterial properties of PBAT and PBAT/LNP-8 composite were investigated, and the results are shown in Figure 12. The colony numbers of *E. coli* and *S. aureus* in the PE group were comparable to those of the control group, indicating that PBAT hardly had any antibacterial property. However, the colony numbers of *E. coli* and *S. aureus* in the PBAT/LNP-8 group were significantly less than those of the control group, suggesting that the incorporation of LNP effectively enhanced the antibacterial property of the composites. It is ascribed to the fact that polyphenols caused damage in the cell wall via lysis, resulting in the leakage of the internal fluid [49]. Furthermore, there were numerous reactive oxygen

species. They were absorbed by the polyphenol compounds, aggregating on the surface of LNP because of its high anti-oxidation behavior. It could release and induce oxidative stress by altering the normal redox physiological process through contacting the bacteria [50].

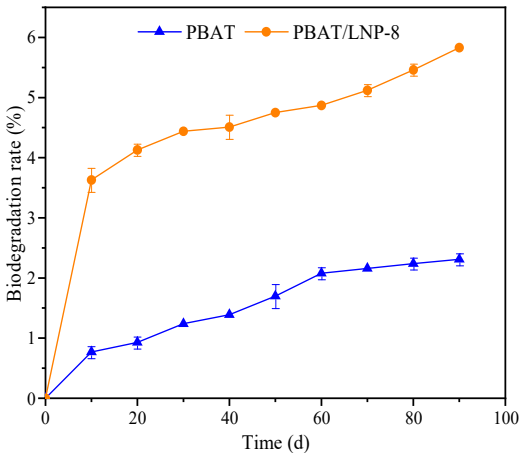


Figure 11. Biodegradation rate of PBAT and PBAT/LNP-8.

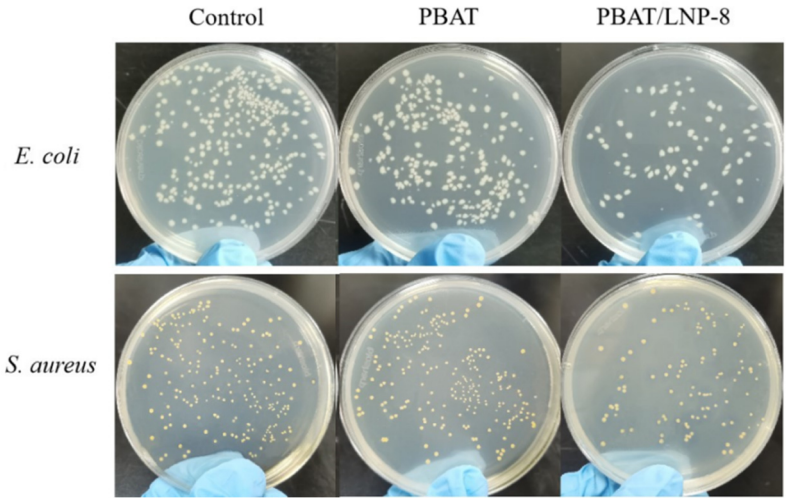


Figure 12. Antibacterial properties of PBAT and PBAT/LNP-8.

3.2.8. Comparison of the Properties

The comprehensive properties of the PBAT/LNP-8 composite were compared with CDBP, and the results are shown in Figure S1. Compared with CDBP, PBAT/LNP-8 had similar thermal properties and a slightly smaller WCA, while its mechanical properties, UV-blocking performance, and gas barrier properties were significantly better. It is evident that PBAT/LNP-8 had good comprehensive properties, which met the performance requirements of packaging materials. It is expected to be applied in the field of biodegradable packaging materials, since DL is mainly derived from agricultural waste such as straw and bamboo. Therefore, lignin was further extracted from wheat straw, and the properties of the composite derived from WSL and PBAT (PBAT/WSL) were also determined. The results in Table S2 showed that the mechanical properties, WCA, and gas barrier properties of PBAT/WSL were close to those of the PBAT/LNP-8 composite. These results indicated that the technology developed in this work was universal and can be applied to lignin from different sources and different extraction methods. It is conducive to expanding the application range of lignocellulosic biomass.

4. Conclusions

The PBAT/LNP composite was successfully prepared by blending PBAT and LNP from DL. The mechanical properties, oxygen barrier property, UV-blocking performance, and biodegradation property of the PBAT/LNP composites were improved by the addition of LNP, and PBAT/LNP-8 had the best comprehensive properties. Compared to neat PBAT, the mechanical properties and biodegradation rate increased, and the OP decreased. PBAT/LNP-8 also had good antibacterial properties, and its mechanical properties, UV-blocking performance, and gas barrier properties were significantly better than those of the CDBP. Moreover, the PBAT/WSL composite, by blending PBAT and lignin from wheat straw, had similar properties to the PBAT/LNP composite. Overall, this work expanded the potential application of lignocellulosic biomass in the packing field. It is beneficial to mitigate the environmental pollution caused by the widespread use of non-degradable plastics and the energy crisis caused by the shortage of fossil resources.

Supplementary Materials: The following supporting information can be downloaded at: https://www.mdpi.com/article/10.3390/pr13113507/s1. Figure S1: Comparison of properties of PBAT/LNP: (a) mechanical properties; (b) contact angle; (c) UV-blocking performance; (d) thermal properties; (e) gas barrier properties. Table S1: Crystallinity of PBAT and its composite. Table S2: Comparison of properties of the composite derived from different lignins [5,17,20,22].

Author Contributions: Formal analysis, Y.L. and T.F.; investigation, Y.L., T.F., and J.L.; writing—original draft, Y.L. and T.F.; data curation, J.L.; writing–review and editing, C.P. and G.F.; methodology, Y.W. and G.F.; project administration, Z.W.; resources, Z.W. and G.F.; supervision, Z.W. and G.F.; conceptualization, G.F.; funding acquisition, G.F. All authors have read and agreed to the published version of the manuscript.

Funding: This research funded by the key project of Hubei Province (2022BCA081).

Data Availability Statement: The original contributions presented in the study are included in the article/Supplementary Material. Further inquiries can be directed to the corresponding author.

Conflicts of Interest: The authors declare that they have no known competing financial interests or personal relationships that could have appeared to influence the work reported in this paper.

References

1. Xiao, L.; Yao, Z.; He, Y.; Han, Z.; Zhang, X.; Li, C.; Xu, P.; Yang, W.; Ma, P. Antioxidant and antibacterial PBAT/lignin-ZnO nanocomposite films for active food packaging. *Ind. Crop. Prod.* **2022**, *187*, 115515. [CrossRef]
2. Ferreira, F.V.; Cividanes, L.S.; Gouveia, R.F.; Lona, L.M.F. An overview on properties and applications of poly(butylene adipate-*co*-terephthalate)-PBAT based composites. *Polym. Eng. Sci.* **2019**, *59*, E7–E15. [CrossRef]
3. Cheng, Z.; Ning, M.; Mao, K.; Nong, X.; Li, J.; Xiao, N.; Zhang, X.; Ding, Q.; Wang, H.; Liu, M. Bamboo powder lignocellulose/polybutylene adipate terephthalate biodegradable bioplastic composite film for food packaging materials. *Int. J. Biol. Macromol.* **2025**, *316*, 144781. [CrossRef]
4. Bilal, M.; Qamar, S.A.; Qamar, M.; Yadav, V.; Taherzadeh, M.J.; Lam, S.S.; Iqbal, H.M.N. Bioprospecting lignin biomass into environmentally friendly polymers-applied perspective to reconcile sustainable circular bioeconomy. *Biomass Convers. Biorefin.* **2022**, *14*, 4457–4483. [CrossRef]
5. Chen, Y.; Feng, T.; Long, Y.; Pan, C.; Fan, G.; Bai, J.; Song, G. Cellulose acetate oleate-reinforced poly(butylene adipate-*co*-terephthalate) composite materials. *e-Polymers* **2023**, *23*, 20230145. [CrossRef]
6. Fan, G.; Peng, Q.; Chen, Y.; Long, Y.; Bai, J.; Song, G.; Cheng, Q. Preparation of biodegradable composite films based on carboxymethylated holocellulose from wheat straw. *Int. J. Biol. Macromol.* **2023**, *242*, 124868. [CrossRef] [PubMed]
7. Peng, Q.; Chen, Y.; Fan, G.; Song, G.; Cheng, Q. Acetylation of wheat straw holocellulose for a biodegradable film. *Cellulose* **2023**, *30*, 8997–9012. [CrossRef]
8. Chen, M.; Li, Y.; Liu, H.; Zhang, D.; Shi, Q.S.; Zhong, X.Q.; Guo, Y.; Xie, X.B. High value valorization of lignin as environmental benign antimicrobial. *Mater. Today Bio* **2022**, *118*, 100520. [CrossRef] [PubMed]

9. Xiong, S.J.; Zhou, S.J.; Wang, H.H.; Wang, H.M.; Shen, X.J.; Yu, S.; Li, H.; Zheng, L.; Wen, J.L.; Yuan, T.Q.; et al. A strong, tough and cost-effective biodegradable PBAT/lignin composite film via intrinsic multiple noncovalent interactions. *Green Chem.* **2023**, *25*, 3175–3186. [CrossRef]
10. Mo, J.; Wang, H.; Yan, M.; Huang, J.; Li, R.; Sun, D.; Lei, J.; Qiu, X.; Liu, W. Construction of interfacial dynamic bonds for high performance lignin/polymer biocompositess. *Front. Chem. Sci. Eng.* **2023**, *17*, 1372–1388. [CrossRef]
11. Li, W.; Huang, J.; Liu, W.; Qiu, X.; Lou, H.; Zheng, L. Lignin modified PBAT composites with enhanced strength based on interfacial dynamic bonds. *J. Appl. Polym. Sci.* **2022**, *139*, e52476. [CrossRef]
12. Liu, Y.; Liu, S.; Liu, Z.; Lei, Y.; Jiang, S.; Zhang, K.; Yan, W.; Qin, J.; He, M.; Qin, S.; et al. Enhanced mechanical and biodegradable properties of PBAT/lignin composites via silane grafting and reactive extrusion. *Compos. Part B-Eng.* **2021**, *220*, 108980. [CrossRef]
13. Olonisakin, K.; Wen, A.; He, S.; Lin, H.; Tao, W.; Chen, S.; Lin, W.; Li, R.; Zhang, X.; Yang, W. The development of biodegradable PBAT-lignin-tannic acid composite film: Properties, biodegradability, and potential barrier application in food packaging. *Food Bioprocess. Technol.* **2023**, *16*, 1525–1540. [CrossRef]
14. Zhu, B.; Xu, Y.; Xu, H. Preparation and application of lignin nanoparticles: A review. *Nano Futures* **2022**, *6*, 032004. [CrossRef]
15. Ainali, N.M.; Tarani, E.; Zamboulis, A.; Črešnar, K.P.; Zemljič, L.F.; Chrissafis, K.; Lambropoulou, D.A.; Bikiaris, D.N. Thermal stability and decomposition mechanism of PLA nanocomposites with kraft lignin and tannin. *Polymers* **2021**, *13*, 2818. [CrossRef] [PubMed]
16. Makri, S.P.; Xanthopoulou, E.; Klonos, P.A.; Grigoropoulos, A.; Kyritsis, A.; Tsachouridis, K.; Bikiaris, D.N. Effect of micro-and nano-lignin on the thermal, mechanical, and antioxidant properties of biobased PLA-lignin composite films. *Polymers* **2022**, *14*, 5274. [CrossRef] [PubMed]
17. Huang, J.; Guo, Q.; Zhu, R.; Liu, Y.; Xu, F.; Zhang, X. Facile fabrication of transparent lignin sphere/PVA nanocomposite films with excellent UV-shielding and high strength performance. *Int. J. Biol. Macromol.* **2021**, *189*, 635–640. [CrossRef]
18. Wang, Z.; Li, C.; Liu, X.; Jia, W.; Huang, L.; Wu, L.; Fatehi, P.; Shi, H. Fabrication and Performance of PBAT Composite Films Reinforced with High-Molecular-Weight Lignin Nanoparticles for Sustainable Packaging. *ACS Sustain. Chem. Eng.* **2025**, *13*, 13740–13752. [CrossRef]
19. Botta, L.; Titone, V.; Teresi, R.; Scarlata, M.C.; Lo Re, G.; La Mantia, F.P.; Lopresti, F. Biocomposite PBAT/lignin blown films with enhanced photo-stability. *Int. J. Biol. Macromol.* **2022**, *217*, 161–170. [CrossRef]
20. Yu, B.; Fan, G.; Zhao, S.; Lu, Y.; He, Q.; Cheng, Q.; Song, G. Simultaneous isolation of cellulose and lignin from wheat straw and catalytic conversion to valuable chemical products. *Appl. Biol. Chem.* **2021**, *64*, 15. [CrossRef]
21. Long, H.; Hu, L.; Yang, F.; Cai, Q.; Zhong, Z.; Zhang, S.; Guan, L.; Xiao, D.; Zheng, W.; Zhou, W.; et al. Enhancing the performance of polylactic acid composites through self-assembly lignin nanospheres for fused deposition modeling. *Compos. Part B Eng.* **2022**, *239*, 109968. [CrossRef]
22. Li, H.; Li, F.; Wang, L.; Sheng, J.; Xin, Z.; Zhao, L.; Xiao, H.; Zheng, Y.; Hu, Q. Effect of nano-packing on preservation quality of Chinese jujube (Ziziphus jujuba Mill. var. inermis (Bunge) Rehd. *Food Chem.* **2009**, *114*, 547–552. [CrossRef]
23. *ISO 527-4-2021*; Test Conditions for Isotropic and Orthotropic Fibre-Reinforced Plastic Composite. ISO: Geneva, Switzerland, 2021.
24. *ASTM E-96-95*; Standard Test Methods for Water Vapor Transmission of Materials. ASTM: West Conshohocken, PA, USA, 1995.
25. Pinheiro, I.F.; Ferreira, F.V.; Souza, D.H.S.; Gouveia, R.F.; Lona, L.M.F.; Morales, A.R.; Mei, L.H.I. Mechanical., rheological and degradation properties of PBAT nanocomposites reinforced by functionalized cellulose nanocrystals. *Eur. Polym. J.* **2017**, *97*, 356–365. [CrossRef]
26. Quan, X.; Ma, J.; Sun, L.; Huang, G.; Sui, S.; Li, H.; Shao, Q.; Yan, S.; Wang, Y.; Wang, X. Enhanced functional properties of chitosan films incorporated with proanthocyanidins/cinnamaldehyde/γ-cyclodextrin microcapsules for citrus fruit preservation. *J. Food Process. Preserv.* **2025**, *2025*, 7504108. [CrossRef]
27. Zhao, Y.; Zhou, S.; Xia, X.; Tan, M.; Lv, Y.; Cheng, Y.; Tao, Y.; Lu, J.; Du, J.; Wang, H. High-performance carboxymethyl cellulose-based hydrogel film for food packaging and preservation system. *Int. J. Biol. Macromol.* **2022**, *223*, 1126–1137. [CrossRef] [PubMed]
28. Lin, X.; Chen, L.; Li, H.; Lv, Y.; Liu, Y.; Lu, X.; Liu, M. Mild depolymerization of the sinocalamus oldhami alkali lignin to phenolic monomer with base and activated carbon supported nickel-tungsten carbide catalyst composite system. *Bioresour. Technol.* **2021**, *333*, 125136. [CrossRef]
29. Yu, H.; Wang, B.; Wang, Y.; Xu, E.; Wang, R.; Wu, S.; Wu, W.; Ji, B.; Feng, X.; Xu, H.; et al. Lignin nanoparticles with high phenolic content as efficient antioxidant and sun-blocker for food and cosmetics. *ACS Sustain. Chem. Eng.* **2023**, *11*, 4082–4092. [CrossRef]
30. Liu, C.; Li, Y.; Hou, Y. A simple environment-friendly process for preparing high-concentration alkali lignin nanospheres. *Eur. Polym. J.* **2019**, *112*, 15–23. [CrossRef]
31. Zhang, J.; Tian, Z.; Ji, X.; Zhang, F. Fabrication mechanisms of lignin nanoparticles and their ultraviolet protection ability in PVA composite film. *Polymers* **2022**, *14*, 4196. [CrossRef]

32. Cai, Y.; Lv, J.; Feng, J. Spectral characterization of four kinds of biodegradable plastics: Poly (lactic acid), poly (butylenes adipate-co-terephthalate), poly (hydroxybutyrate-co-hydroxyvalerate) and poly (butylenes succinate) with FTIR and raman spectroscopy. *J. Polym. Environ.* **2013**, *21*, 108–114. [CrossRef]
33. Mohanty, S.; Nayak, S.K. Biodegradable nanocomposites of poly(butylene adipate-co-terephthalate) (PBAT) and organically modified layered silicates. *J. Polym. Environ.* **2012**, *20*, 195–207. [CrossRef]
34. Cichosz, S.; Masek, A.I.R. study on cellulose with the varied moisture contents: Insight into the supramolecular structure. *Materials* **2013**, *13*, 4573. [CrossRef] [PubMed]
35. Wang, Y.; Hou, Y.; Wu, W.; Li, H.; Ren, S.; Li, J. Polycyclic aromatics observed in enzymatic lignin by spectral characterization and ruthenium ion-catalyzed oxidation. *J. Agric. Food Chem.* **2021**, *69*, 12148–12155. [CrossRef] [PubMed]
36. Barros, J.J.P.; Oliveira, R.R.; Luna, C.B.; Wellen, R.M.; Moura, E.A.B. Effectiveness of modified lignin on poly(butylene adipate-co-terephthalate)/poly(lactic acid) mulch film performance. *J. Appl. Polym. Sci.* **2023**, *140*, 54684. [CrossRef]
37. Gu, X.; Hou, J.; Ai, S. Effect of silane modified nano-SiO_2 on the mechanical properties and compatibility of PBAT/lignin composite films. *J. Appl. Polym. Sci.* **2021**, *139*, 52051. [CrossRef]
38. Ferreira, R.R.; Souza, A.G.; Barbosa, R.F.S.; Marciano, J.S.; Marques, F.A.S.; Mitra, S.K.; Rosa, D.S. The synergistic effect of nanocellulose and nanocapsules into poly(butylene adipate-co-butylene terephthalate) films for active packaging. *Polymer* **2020**, *35*, 100996. [CrossRef]
39. Kargarzadeh, H.; Galeski, A.; Pawlak, A. PBAT green composites: Effects of kraft lignin particles on the morphological, thermal, crystalline, macro and micromechanical properties. *Polymer* **2020**, *203*, 122748. [CrossRef]
40. Giteru, S.G.; Ali, A.; Oey, I. Understanding the relationship between rheological characteristics of pulsed electric fields treated chitosan-zein-poly(vinyl alcohol)-polyethylene glycol composite dispersions and the structure-function of their resulting thin-films. *Food Hydrocoll.* **2021**, *113*, 106452. [CrossRef]
41. Zou, Z.; Ismail, B.; Zhang, X.; Yang, Z.; Liu, D.; Guo, M. Improving barrier and antibacterial properties of chitosan composite films by incorporating lignin nanoparticles and acylated soy protein isolate nanogel. *Food Hydrocoll.* **2023**, *134*, 108091. [CrossRef]
42. Ge, X.; Chang, M.; Jiang, W.; Zhang, B.; Xing, R.; Bulin, C. Investigation on two modification strategies for the reinforcement of biodegradable lignin/poly(lactic acid) blends. *J. Appl. Polym. Sci.* **2020**, *137*, 49354. [CrossRef]
43. Wang, H.M.; Wang, B.; Yuan, T.Q.; Zheng, L.; Shi, Q.; Wang, S.F.; Sun, R.C. Tunable, UV-shielding and biodegradable composites based on well-characterized lignins and poly(butylene adipate-*co*-terephthalate). *Green Chem.* **2020**, *22*, 8623–8632. [CrossRef]
44. Xiong, S.J.; Zhou, S.J.; Wang, H.H.; Wang, H.M.; Yu, S.; Zheng, L.; Yuan, T.Q. Fractionation of technical lignin and its application on the lignin/poly-(butylene adipate-*co*-terephthalate) bio-composites. *Int. J. Biol. Macromol.* **2022**, *209*, 1065–1074. [CrossRef]
45. Li, Y.; Li, F.; Yang, Y.; Ge, B.; Meng, F. Research and application progress of lignin-based composite membrane. *J. Polym. Eng.* **2021**, *41*, 245–258. [CrossRef]
46. Siracusa, V. Food packaging permeability behaviour: A report. *Int. J. Polym. Sci.* **2012**, *2012*, 302029. [CrossRef]
47. Kim, J.; Bang, J.; Park, S.; Jung, M.; Jung, S.; Yun, H.; Kim, J.H.; Choi, I.G.; Kwak, H.W. Enhanced barrier properties of biodegradable PBAT/acetylated lignin films. *Sustain. Mater. Technol.* **2023**, *7*, e00686. [CrossRef]
48. Xing, Q.; Buono, P.; Ruch, D.; Dubois, P.; Wu, L.; Wang, W.J. Biodegradable UV-blocking films through core–shell lignin–melanin nanoparticles in poly(butylene adipate-*co*-terephthalate). *ACS Sustain. Chem. Eng.* **2019**, *7*, 4147–4157. [CrossRef]
49. Yang, W.; Fortunati, E.; Gao, D.; Balestra, G.M.; Giovanale, G.; He, X.; Torre, L.; Kenny, J.M.; Puglia, D. Valorization of acid isolated high yield lignin nanoparticles as innovative antioxidant/antimicrobial organic materials. *ACS Sustain. Chem. Eng.* **2018**, *6*, 3502–3514. [CrossRef]
50. He, Y.; Li, H.; Fei, X.; Peng, L. Carboxymethyl cellulose/cellulose nanocrystals immobilized silver nanoparticles as an effective coating to improve barrier and antibacterial properties of paper for food packaging applications. *Carbohydr. Polym.* **2021**, *252*, 117156. [CrossRef] [PubMed]

Disclaimer/Publisher's Note: The statements, opinions and data contained in all publications are solely those of the individual author(s) and contributor(s) and not of MDPI and/or the editor(s). MDPI and/or the editor(s) disclaim responsibility for any injury to people or property resulting from any ideas, methods, instructions or products referred to in the content.